PHYSICAL REVIEW B **80**, 235417 (2009)

Theory of the magnetic-field-induced insulator in neutral graphene sheets

J. Jung and A. H. MacDonald
Department of Physics, University of Texas at Austin, Austin, Texas 78712, USA
(Received 7 September 2009; revised manuscript received 30 October 2009; published 10 December 2009)

Recent experiments have demonstrated that neutral graphene sheets have an insulating ground state in the presence of an external magnetic field. We report on a π-band tight-binding-model Hartree-Fock calculation which examines the competition between distinct candidate insulating ground states. We conclude that for graphene sheets on substrates the ground state is most likely a field-induced spin-density wave and that a charge-density-wave state is possible for suspended samples. Neither of these density-wave states support gapless edge excitations.

DOI: 10.1103/PhysRevB.80.235417 PACS number(s): 73.63.−b, 73.43.−f, 71.10.Pm, 73.21.−b

I. INTRODUCTION

The magnetic band-energy quantization properties of graphene sheets lead to quantum-Hall effects[1–3] (QHEs) with $\sigma_{xy}=\nu e^2/h$ at filling factors $\nu=4(n+1/2)=\ldots,-6,-2,2,6,\ldots$ for any integer value of n. The factor of 4 in this expression accounts for a graphene sheet's twofold valley and spin degeneracies. When Zeeman spin splitting of Landau levels is included, quantum-Hall effects are expected at the remaining even integer values of ν, including the neutral graphene $\nu=0$ case. The $\nu=0$ quantum-Hall effect of neutral graphene systems is interesting from two different points of view. First of all, the transport phenomenology of the quantum-Hall effect[3] is different at $\nu=0$ because of the possible absence of edge states. Indeed the initial experimental indications[3] that a $\nu=0$ quantum-Hall effect occurs in neutral graphene did not exhibit either the clear plateau in ρ_{xy} or the deep minimum in ρ_{xx} which are normally characteristic of the QHE. Second, although a quantum-Hall effect is expected at $\nu=0$ even for noninteracting electrons, the large energy gaps identified experimentally suggest that interactions play a substantial role in practice. Gaps due entirely to electron-electron interactions in ordered states are in fact common[4,5] in quantum-Hall systems when two or more Landau levels are degenerate. Partly for this reason, a number of different scenarios have been proposed[6–16] in which the gap at $\nu=0$ is associated with different types of broken symmetry within the four quasidegenerate Landau levels near the Fermi level of a neutral graphene sheet. The prevailing view has been that the ground state is spin polarized, with partial filling factors ν_σ equal to 1 and −1 for majority and minority spins, respectively. This state has an interesting edge-state structure identical to that of quantum-spin-Hall systems,[17] and transport properties in the quantum-Hall regime that are controlled by the properties of current-carrying spin-resolved chiral edge states.[8,18]

The simplest picture of strong-field physics in nearly neutral graphene sheets is obtained by using the Dirac-equation continuum model and neglecting interaction-induced mixing between Landau levels with different principal quantum number n. In this model, electron-electron interactions are valley and spin dependent. When Zeeman interactions and disorder are neglected, the broken-symmetry ground state consists[12] of two-filled $n=0$ Landau levels with arbitrary spinors in the four-dimensional spin-valley space. This family of states is favored by electron-electron interactions because of Fermi statistics which lowers Coulomb-interaction energies when the orbital content of electrons in the fermion sea is polarized. When Zeeman coupling is included, it uniquely selects from this family the state in which both $n=0$ valley orbitals are occupied for majority-spin states and empty for minority-spin states. The interacting system ground state is then identical to the noninteracting-system ground state, although interactions are expected[12] to dramatically increase the energy gap for charged excitations.

This argument for the character of the ground state appears to be compelling but its conclusions are nevertheless uncertain. First of all, Landau-level mixing effects are normally stronger than Zeeman interactions, and could play a role.[19] In addition, although corrections[7,9–11,20] to the continuum model for graphene are known to be small at experimental field strengths, they could still be more important than the Zeeman interactions. Suspicions that the character of the ground state could be misrepresented by the $n=0$ continuum-model theory have been heightened recently by the work of Ong and collaborators, who found a steep increase in the Dirac-point resistance[21] with magnetic field and evidence for a field-induced transition to a strongly insulating state at a finite magnetic-field strength.[22] Somewhat less dramatic increases in resistance at the Dirac point have also been reported by other researchers.[23–25]

In this paper we attempt to shed light on the ground state of neutral graphene in a magnetic field by performing self-consistent Hartree-Fock calculations for a π-orbital tight-binding model. In the continuum model, Hartree-Fock theory is known[12] to yield the correct ground state. By using a π-orbital tight-binding model we can at the same time conveniently account for Landau-level mixing effects and systematically account for lattice corrections to the Dirac-equation continuum model. As we will discuss at length below, it is essential to perform the mean-field-theory calculations with Coulombic electron-electron interactions and not the Hubbard-type interactions commonly used[10,26] with lattice models. One disadvantage of our approach is that our calculations are feasible only at magnetic-field strengths which are stronger than those available experimentally. We therefore carefully examine the dependence on magnetic-field strength and extrapolate to weaker fields. We conclude

that under typical experimental conditions the most-likely field-induced state of neutral graphene on a SiO_2 substrate is a spin-density-wave state, and that suspended samples might have a charge-density-wave state. Neither of these orderings support edge states in the $\nu=0$ gap. We also discuss the magnetic-field dependence of different contributions to the total energy and estimate a critical value of perpendicular and tilted magnetic field at which Zeeman splitting will bring about a phase transition to a solution with net spin polarization which *does* support edge states.

Although our calculation captures some realistic features of graphene sheets that are neglected in continuum models, it is still not a complete *all-electron* many-body theory. In particular, we neglect the carbon σ and σ^* orbitals whose polarization is expected to screen the Coulomb interactions at short distances. Because of our uncertainty as to the strength of this screening, our conclusions cannot be definitive. We nevertheless hope that our calculations, in combination with experiment, will prove useful in identifying the character of the field-induced insulating state in neutral graphene.

Our paper is organized as follows. In Sec. II we explain in detail the model which we study which has two parameters, a relative dielectric constant ε_r which accounts for the dielectric environment of the graphene sheet, and the on-site interaction U which accounts for short-distance screening effects, for example, by σ-band polarization. Our main results on the competition between different ordered states are presented in Sec. III. In Sec. IV we turn to a discussion of the electronic structure of neutral graphene ribbons, paying particular attention to their edge states which play a key role in most quantum-Hall transport experiments. Finally in Sec. V we summarize our main conclusions.

II. INTERACTING-ELECTRON LATTICE MODEL FOR GRAPHENE SHEETS

A. Noninteracting electron π-band model

We first comment briefly on the π-band tight-binding model of graphene in the presence of a magnetic field.[27–31] Each carbon atom on graphene's honeycomb lattice has three near neighbors with π-orbital hopping parameter $t=-2.6$ eV. Magnetic-field effects are captured by a phase factor in the hopping amplitudes: $t \to t \times e^{2\pi i \phi}$, where $\phi = (e/ch)\int \mathbf{A} d\mathbf{l}$ depends on line integral of the vector potential $\mathbf{A}$ along a trajectory linking the two lattice sites. When the dimensionless magnetic-flux density is $\phi \equiv BS_{hex}/\phi_0 = 1/q$, where q is an integer and $\phi_0 = ch/e$ is a magnetic-flux quantum, it is possible to apply Bloch's theorem in a unit cell which is enlarged by a factor of q relative to the honeycomb lattice unit cell. (The honeycomb lattice unit-cell area $S_{hex} = \sqrt{3}a^2/2$ and $a=2.46$ Å for a graphene sheet.) Lattice-model Landau levels have a small width which increases with magnetic-field strength and reflects magnetic breakdown effects neglected in the continuum model.

The ground-state energy-density differences discussed below scale approximately as powers of the magnetic length ℓ_B, defined by $2\pi\ell_B^2 B = \phi_0$. (ℓ_B and q are related by $\ell_B = (S_{hex}q/2\pi)^{1/2} = 0.371\sqrt{q}a = 0.913\sqrt{q}$ Å.) In a continuum-model description the density contributed by a single full Landau level is $1/2\pi\ell_B^2$ and the energy of the nth Landau level is given by $E_n = \pm 2\hbar v_F \sqrt{|n|}/\ell_B$, where $v_F = \sqrt{3}at/2\hbar$ is the Fermi velocity of graphene. All energy levels evolve with magnetic field except for the $n=0$ level, $E_0=0$.[32] When the nth Landau level is full it contributes $E_n/(2\pi\ell_B^2)$ to the energy density. From this we immediately see that in the weak-field limit important energies tend to scale as $\ell_B^{-3} \propto B^{3/2}$. It is easy to show, for example, that the magnetic-field dependence of the total band energy of a neutral noninteracting graphene sheet is given by $E(\ell_B) = a_{kin}/\ell_B^3$, where $a_{kin} = 2.6$ eV Å^3. This nonanalytic field dependence is responsible for the divergent weak-field diamagnetic response $[(\partial E_{tot}/\partial B)/B]$ of graphene discussed some time ago by McClure.[33] We show below that when interactions are included, the energy differences between competing field-induced insulator states also tend to vary as ℓ_B^{-3}.

B. π-band model effective interactions

It is clear from previous analysis of lattice corrections to continuum models[7,9–11,20] and from lattice-model calculations based on extended Hubbard models[10] that conclusions on the nature of the field-induced insulating ground state are very dependent on the effective electron-electron interactions used in a π-band lattice model of graphene. In particular, it seems clear that the long-range $1/r$ Coulomb interaction tail is essential. We approximate the interaction between π orbitals located at sites separated by a distance d by $V(d) = 1/(\varepsilon_r\sqrt{a_o^2+d^2})$, where $a_o = a/(2\sqrt{3})$, the bonding radius of the carbon atoms, accounts approximately for interaction reduction due to π-charge smearing on each lattice site,[34] and ε_r accounts for screening due to the dielectric environment of the graphene sheet. (Here energies are in Hartree (e^2/a_B) units and lengths are in units of the Bohr radius a_B.) The on-site repulsive interaction parameter, U, is not well known and we take it to be a separate parameter. We motivate the range of values considered for this interaction parameter below. The value chosen for ε_r can also represent in part screening by σ orbitals neglected in our approximation or be understood as an *ad hoc* correction for overestimates of exchange interactions in Hartree-Fock theory. Although we study a range of values for this interaction parameter model in order to test the robustness of our conclusions, we believe that a value of $\varepsilon_r \sim 4$ is normally appropriate for graphene sheets placed on a dielectric substrate. For practical reasons we truncate the range of Coulomb interaction in real space at $d = L_{\max} = 6.5a$. This type of truncation is especially helpful when treating systems without periodic boundary conditions and allows us to avoid problems due to slowly converging sums in real space that can otherwise be treated through the Ewald sum method.[35] Truncation of the Coulomb interaction at a reasonably large $L_{\max}$ must however be applied with utmost care in order to obtain solutions consistent[36,37] with the limit $L_{\max} \to \infty$.

In considering appropriate values for the on-site interaction U we can start from the Coulomb-interaction energy at the carbon radius length scale which is ~ 20 eV while this estimate can be reduced if one considers a charge distribution corresponding to a p orbital. In fact an estimate from the

first ionization energy and electron affinity gives $U=9.6$ eV.[38] It is known that the effective on-site interaction strength is greatly reduced from this bare value in the solid-state environment because of screening by polarization of bound orbitals on nearby carbon atoms. We consider values of U between 2 and 6 eV, bracketing values deemed appropriate by a variety of different researchers.[7,39–41] A larger value of U increases the interaction energy cost of any charge-density-wave (CDW) state which might occur. The direct-interaction energy is zero when all carbon sites stay neutral but can be positive or negative in CDW states. In the CDW states we discuss below electron density δn is transferred between A and B honeycomb sublattices. In this state the direct-interaction energy per site is

$$\delta E_{DI} = \frac{(\delta n)^2}{2}\left[U + \sum_{j\in A} V(d_{ij}) - \sum_{j\in B} V(d_{ij})\right], \qquad (1)$$

where d_{ij} is the distance between lattice sites i and j, $U=V(d_{ii})$ and i is a fixed label belonging to sublattice A. The largest terms in Eq. (1) are the repulsive on-site interactions which are proportional in our model to U and attractive excitonic interaction between electrons on neighboring opposite sublattice sites which are inversely proportional to ε_r. Using an Ewald technique to sum over distant sites we find that δE_{DI} is positive for $\varepsilon_r U > 13.05$ eV . (The corresponding criterion for the truncated Coulomb interactions we use in our self-consitent-field calculations is $\varepsilon_r U >= 12.23$ eV; the difference between the right-hand side of these two equations is one indicator of the inaccuracy introduced by truncating the Coulomb interaction.) When $\varepsilon_r U < 12.23$ eV the CDW state is stable unless band and exchange energies support a uniform-density state.[37]

Given the band-structure model and the interaction model, the Hartree-Fock mean-field-theory calculations for bulk graphene sheets with periodic boundary conditions and for graphene ribbons reported in the following sections are completely standard.[42] The band quasiparticles are determined by diagonalizing a single-particle Hamiltonian which includes direct- and exchange-interaction terms. The direct and exchange potentials are expressed in terms of the occupied quasiparticle states and must be determined self-consistently. (We do not quote the detailed expressions for these terms here.) Since the Hartree-Fock equations can be derived by minimizing the total energy for single Slater-determinant wave functions, every solution we find corresponds to an extremum of energy. The iteration procedure is stable only if the extremum is a minimum so we can be certain that all the solutions found below represent local energy minima among single Slater-determinant wave functions with the same symmetry properties.

III. FIELD-INDUCED INSULATING GROUND STATES

A. Identification of candidate states

At zero-field band energy favors neutral graphene states without broken symmetries and there is no compelling evidence from experiment that they are induced by interactions. In a perpendicular magnetic field, however, the systems is particularly susceptible to the formation of broken-symmetry ground states because of the presence of a half-filled set of fourfold spin (neglecting Zeeman) and valley degenerate Landau levels with (essentially) perfectly quenched band energy. Although the final ground-state selection probably rests on considerations that it fails to capture, the $n=0$ continuum model captures the largest part of the interaction energy and most of the qualitative physics. The ground state is formed by occupying two of the four $n=0$ Landau levels, selected at random from the four-dimensional orbital space, and producing a gap for charged excitations.

Three representative broken-symmetry states are illustrated in Fig. 1. Because $n=0$ Landau-level orbitals associated with different valleys are completely localized on different honeycomb sublattices, a CDW solution results when $n=0$ orbitals are occupied for both spins of one valley. (When Landau-level mixing is neglected valley indices and A or B sublattice indices are equivalent.) This state lowers the translational symmetry of the honeycomb lattice in a way which removes inversion symmetry. The other extreme is a spontaneously spin-polarized uniform-density state (ferromagnetic—F) in which $n=0$ orbitals are occupied in both valleys but only for one spin component. A third type of broken-symmetry state, the spin-density-wave (SDW) state, has both broken inversion symmetry and broken spin-rotational invariance. In the cartoon version of Fig. 1, $n=0$ electrons occupy states with one spin orientation on one sublattice and the opposite spin orientation on the other sublattice. Possible broken-symmetry states, some at other filling factors, had been discussed previously by several authors.[7,10] These three states are all contained within the $n=0$ continuum-model family of ground states whose degeneracy is lifted by lattice and Landau-level mixing effects. In the self-consistent mean-field-theory calculations described in detail below, the three states identified above all appear as energy extrema in our collinear-spin study.

B. Energy comparisons

In order to examine the physics behind the competition between the candidate ground states we decompose the total energy for all three contributions into band, direct-interaction, and exchange-interaction contributions. We have obtained self-consistent solutions for all three states over a range of on-site interaction U and the dielectric screening ε_r values. Because of kinetic-energy quenching in the (essentially degenerate) $n=0$ Landau level, the interaction strengths required to drive the system into an ordered state are essentially zero. The key question, then, is which state is favored. In Fig. 1 we illustrate how the energy differences between the three states depend on the model interaction parameters. The results in this figure were obtained for $q=100$ unit cells per flux quantum, which corresponds to perpendicular field strength $B=792$ T. The unit cells in which we can apply periodic boundary conditions in this case contain 100×2 lattice sites. The k-space integrations in the self-consistent Hartree-Fock calculations were performed using a 60 k-point Brillouin-zone sampling. The self-consistent field equations were iterated until the total energies were converged to nine

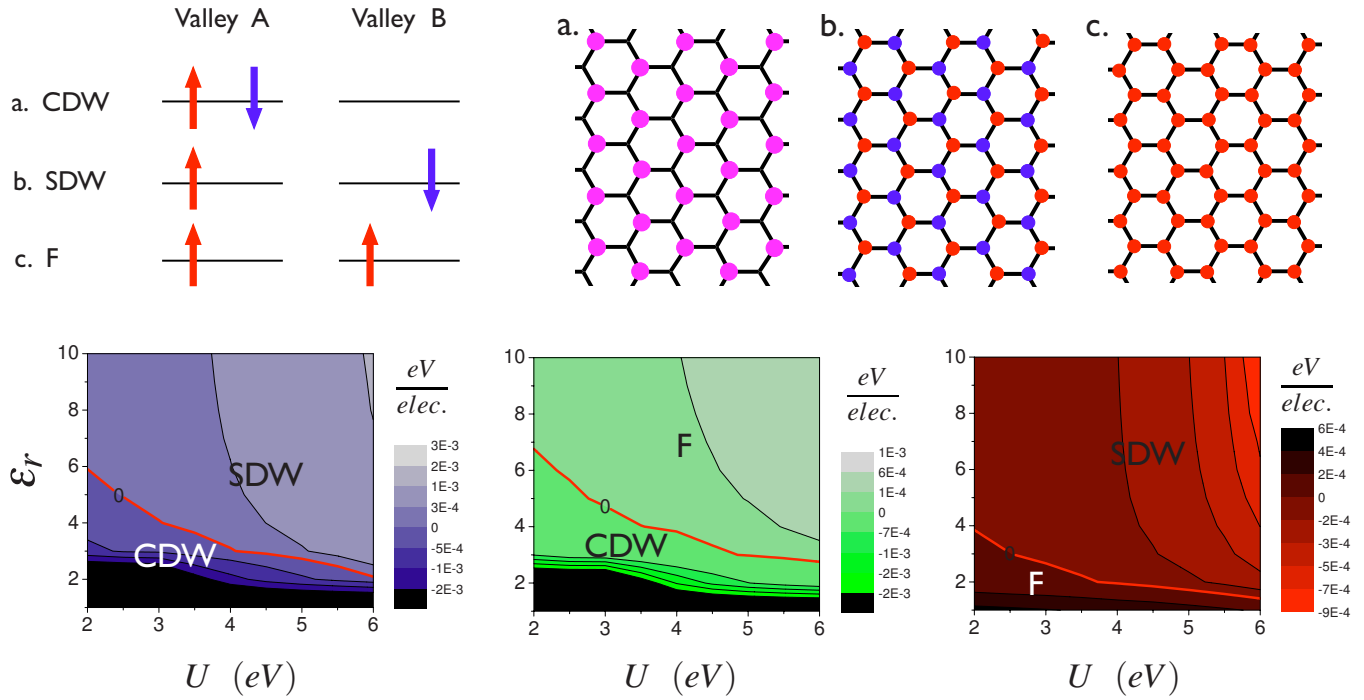

FIG. 1. (Color online) Upper panel: Schematic representation of valley polarized CDW, SDW and F spin-polarized broken-symmetry solutions that can be obtained in a self-consistent mean-field calculation of graphene under a perpendicular magnetic field at half filling. Each arrow represents the filling of one $n=0$ Landau level of a given spin and valley. Lower panel: From left to right $E^{\mathrm{CDW}}-E^{\mathrm{SDW}}$, $E^{\mathrm{CDW}}-E^{\mathrm{F}}$, and $E^{\mathrm{SDW}}-E^{\mathrm{F}}$ total-energy differences per electron in eV as a function of the on-site repulsion U and ε_r obtained from a data mesh of 9 $\times 10$ points, calculated neglecting the Zeeman term and for a magnetic field of 792 T corresponding to 1/100 of a flux quantum per honeycomb hexagon. For smaller values of U the CDW solutions are energetically favored whereas for larger values of U the SDW solutions are favored in a wide range of ε_r. The F solutions are never the lowest in energy. The zero energy red contour lines indicate degeneracy between two different solutions.

significant figures. High accuracy is required because the three states are very similar in energy since the ordering occurs primarily in the $n=0$ Landau level, involving only 1% or so of the electrons for this value of q. This accuracy was sufficient to evaluate energy differences that typically have three significant figures.

The first point to notice in these plots of energy differences is that the two uniform charge-density solutions, the F solution and the SDW solution, behave similarly. The largest contrast therefore is between the CDW solution and the SDW and F solutions. Focusing first on the CDW/SDW comparison we notice that the SDW state is favored when U is large or ε_r is large. The crossover occurs near $\varepsilon_r U \sim 12$ eV, very close to the line along which δE_{DI} changes sign. The fact that the CDW/SDW phase boundary occurs very close to this line is expected because of kinetic-energy quenching in a magnetic field. When the nonuniform-density CDW state is compared with the uniform-density spin-polarized F state the phase boundary moves very close to a larger value of this product with $\varepsilon_r U$ ranging from ~ 14 to ~ 18 eV along the phase boundary. Evidently the competition between CDW and SDW states is based very closely on the direct-interaction energy, with additional weaker elements of the competition entering when the F state is considered.

Direct comparison between the uniform-density SDW and F solutions indicates that the latter is favored only at values of U and ε_r which are outside the range of most-likely values. As discussed in more detail below, we find that the direct-interaction energy in these two states is identical, and that the more negative exchange energy of the SDW state overcomes a larger band energy. In this case the main difference between the energies of the two states arises from Landau-level mixing effects. As we explain later, Landau-level mixing leads to a local spin polarization which is larger in the SDW state than in the F state.

In Fig. 1 we have introduced the main trends in the energetic competition between CDW, SDW, and F states. However, as we have explained, these calculations were undertaken at field strengths that exceed those available experimentally. In the following section we demonstrate that the field dependence of the energy comparisons is extremely systematic so that extrapolations down to physical field strengths are reliable. So far we have also ignored Zeeman coupling which favors F states. This coupling can be important and is also addressed in the following subsection.

C. Field strength and Zeeman-coupling dependence

We now turn our attention to the magnetic-field dependence of the solutions. For this purpose we found self-consistent solutions over a range of magnetic fields for two sets of interaction parameters, $U=5$ eV and $\varepsilon_r=4$ for which the SDW solution has the lowest energy, and $U=5$ eV and

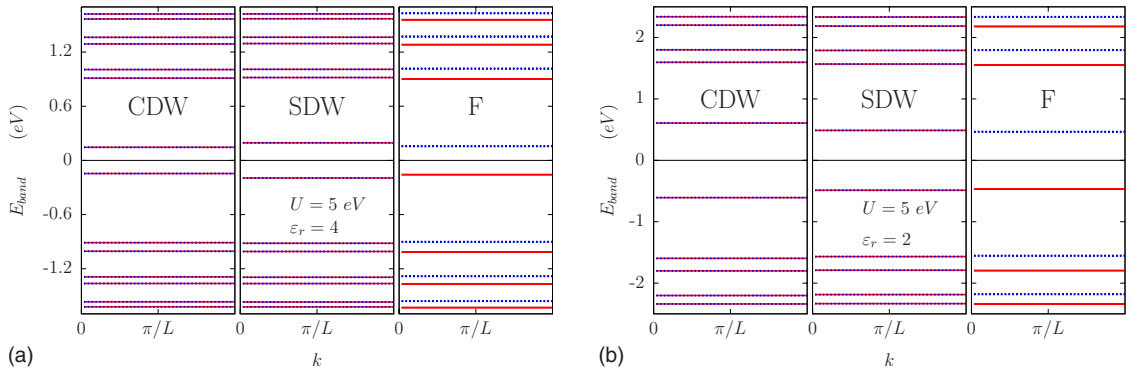

FIG. 2. (Color online) One-dimensional representation of the dispersionless band structure of a graphene sheet under a strong magnetic field $B=440$ T represented in the momentum coordinate k parallel to the narrower direction of the unit cell. The band gaps follow the $B^{1/2}$ scaling law expected from the continuum model. The red color is used to represent up spin while blue is used for down spin. Left Panel: Band structure for CDW, SDW, and F solutions obtained for $U=5$ eV and $\varepsilon_r=4$. For these interaction parameters the SDW state has the lowest energy and the largest gap at the Fermi level. Right Panel: Band structures for $U=5$ eV and $\varepsilon_r=2$. When the on-site repulsion is sufficiently weak the energetically favored solution corresponds to the CDW state and this solution then has the largest gap.

$\varepsilon_r=2$ for which the CDW solution has the lowest energy. The band structures of the different possible solutions for these set of parameters are shown in Fig. 2 and the field dependences of the three energy differences are plotted in Fig. 3. We see that every contribution accurately follows a $B^{3/2} \propto l_B^{-3}$ law with small deviations that can be accounted for by allowing a term proportional to B^2. This is the same field-dependence law that we discussed earlier for the case of a noninteracting electron system. In the continuum model it is guaranteed in neutral graphene when electrons interact via the Coulomb interactions by the fact that both kinetic and interaction energy densities then scale as (length)$^{-3}$; the magnetic field simply provides a scale for measuring density. The fact that we find this field dependence simply shows that the condensation energies of all three ordered states are driven by continuum-model physics. This is in agreement with the intuitive picture of the interaction energy as the product of the number of electrons occupying a Landau level which is directly proportional to B, multiplied by the Coulomb-interaction scale for electrons in the $n=0$ Landau level which is proportional to $B^{1/2}$. The fact that the differences in energy between the three states follows this rule suggests that the most important source of differences in energy between these states is Landau-level mixing, which should not violate the $B^{3/2}$ law. Small deviations from this law are expected because of lattice effects. The deviations are stronger in CDW solutions than in the SDW solutions because of the charge-density inhomogeneity at the lattice scale present in the former.

We can draw two important additional conclusions from the $B^{3/2}$ behavior. First of all, lattice effects are not dominant effect at the field strengths for which we are able to perform calculations, and should be less important at the weaker fields for which experiments are performed because the magnetic length l_B will then be even longer compared to the honeycomb lattice constant. The difference in energy between the three states should mainly vary as $B^{3/2}$ all the way down to zero field, provided only that disorder is negligible. (We discuss the role of disorder again in Sec. V.) Our calculations should therefore reliably predict the energetic ordering of the states in the experimental field range. The second conclusion we can make concerns the importance of Zeeman coupling which we have ignored to this point. First of all,

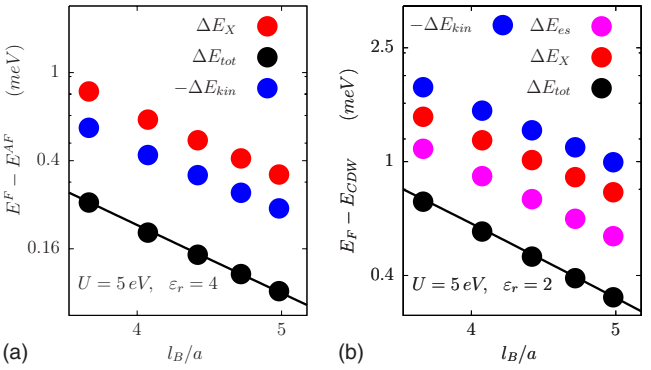

FIG. 3. (Color online) Total energy per site differences ΔE_{tot}, separated into kinetic energy ΔE_{kin}, electrostatic energy ΔE_{DI}, and exchange energy ΔE_{XI} contributions as a function of magnetic length ℓ_B in lattice constant $a=2.46$ Å units. The total-energy differences were fitted to a $C_{3/2}B^{3/2}+C_2B^2$ curve. The fitting parameters are listed in Table I. Left panel: Energy differences between F and SDW solutions $\Delta E^{\mathrm{F/SDW}}=E^{\mathrm{F}}-E^{\mathrm{SDW}}$. These results were obtained with interaction parameter values $U=5$ eV and $\varepsilon_r=4$ for which SDW is the lowest energy configuration. The more negative values of exchange energy in the SDW state compensates the kinetic-energy penalty related to the inhomogeneous accumulation of the electron wave functions at alternating lattice sites. The electrostatic energy differences are zero thanks to the uniform electron density for both solutions. Right panel: Same as the previous figure but for $\Delta E^{\mathrm{F/CDW}}=E^{\mathrm{F}}-E^{\mathrm{CDW}}$. The interaction parameters in this case are $U=5$ eV and $\varepsilon_r=2$ for which CDW is the lowest-energy configuration. When the on-site repulsion U is small enough that the electrostatic energy penalty for the inhomogeneous charge distribution is small, exchange is the main contribution driving the CDW instability. However, in the case illustrated here U is so small that the electrostatic part of the Hamiltonian does play an important role in favoring the CDW state. The energy contributions follow a magnetic-field decay law that deviates more from $B^{3/2}$ than in the previous case because the on-site interaction U plays an essential role.

TABLE I. In the upper table we list the values of $C_{3/2}^{(\mathrm{SDW/CDW})}$ in units of 10^{-10} eV/T$^{3/2}$ and $C_2^{(\mathrm{SDW/CDW})}$ in units of 10^{-10} eV/T^2, obtained from fits to the their energy difference with respect to F states as given in Eq. (2) for two different values of the interaction parameters U and ε_r. The critical field B_c estimates are dependent on the reliability of these fits. Note that a crossover between SDW and CDW states can be driven by changes in the dielectric screening environment captured by ε_r. The lower table lists B_c values at which the F states become critical according to Eq. (3).

	ε_r=2		ε_r=3				ε_r=4			
U	$C_{3/2}^{\mathrm{CDW}}$	C_2^{CDW}	$C_{3/2}^{\mathrm{CDW}}$	C_2^{CDW}	$C_{3/2}^{\mathrm{SDW}}$	C_2^{SDW}	$C_{3/2}^{\mathrm{CDW}}$	C_2^{CDW}	$C_{3/2}^{\mathrm{SDW}}$	C_2^{SDW}
2	NA	NA	322	−1.89			52.6	1.05		
3	NA	NA	130	0			23.2	0.0314		
4	1070	−13.6	54.2	−0.210					51.6	0.0209
5	417	−3.15			111	−0.630			92.8	0.839
6	198	−1.67			255	−2.10			241	0

U	B_C^{CDW}	B_C^{CDW}	B_C^{SDW}	B_C^{CDW}	B_C^{SDW}
2	NA	1200		70	
3	NA	300		10	
4	2600	52			50
5	1600		200		200
6	490		740		1100

Zeeman coupling will have a negligible effect on the energies of the SDW and CDW states since they have a vanishing spin magnetic susceptibility. The energy difference per site between the F state and the two density-wave states can be written in the form

$$\begin{aligned}\Delta E &= E^{(\mathrm{SDW/CDW})} - E^{\mathrm{F}} \\ &= B^{3/2} C_{3/2}^{(\mathrm{SDW/CDW})} \cos(\theta)^{3/2} \\ &\quad + B^2 [C_2^{(\mathrm{SDW/CDW})} \cos(\theta)^2 - C_Z \cos(\theta)] \end{aligned} \tag{2}$$

where B is the total magnetic-field strength and θ is the field tilt angle relative to the graphene plane normal. Factors of $B\cos(\theta)$ in this expression therefore account for the perpendicular field dependence. The second term in Eq. (2) contain the contributions that scale with B^2. The factor of $B\cos(\theta)$ which appears in the Zeeman term is present because the spin polarization of the F state is proportional to the Landau-level degeneracy. The coefficients $C_{3/2}$ and C_2 can be obtained by fitting energy differences obtained from numerical solutions of the self-consistent field equations, like those plotted in Fig. 3, and depend on the interaction model parameters as shown in Table I. The Zeeman coefficient in Eq. (2) is $C_Z = 7.3 \times 10^{-10}$ eV/T^2 is independent of interaction parameters. From the above equation we find that the F state has lower energy than the spin-unpolarized states for

$$B > B_c(\theta) = \frac{C_{3/2}^2 \cos(\theta)}{[C_z - C_2 \cos(\theta)]^2}. \tag{3}$$

The fields required to achieve an energetic preference for the spin-polarized state are smaller at larger tilt angles because the orbital energy has a stronger θ dependence, Fig. 4.

In Table I we show the values of $C_{3/2}$ and C_2 for SDW and CDW configurations favored with respect to F for a set of parameters of U and ε_r. We notice that the coefficients dictating the critical-field transition to F solutions can be made relatively small if the parameters are near the crossover boundary to F states. It is possible that a SDW or CDW to F transition could be induced by varying magnetic field. If a transition was observed, most likely by a change in transport properties as discussed in the next section, it could provide valuable input on the effective interaction parameters of the π-orbital tight-binding model.

IV. QUANTUM-HALL EDGE STATES IN GRAPHENE RIBBONS

The quantum-Hall effect occurs when a two-dimensional (2D) electron system has a chemical-potential discontinuity

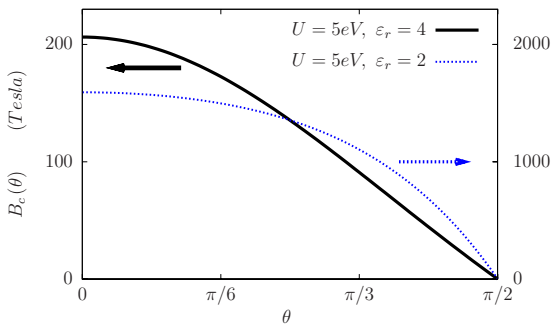

FIG. 4. (Color online) Tilt-angle θ dependence of the critical magnetic field required to induce a transition to the F state. The black solid curve and dashed blue curve represent the critical magnetic fields starting from the SDW and CDW states, respectively. In the CDW curve we observe a larger deviation from a simple $\cos(\theta)$ law due to a stronger influence of lattice scale physics described by the C_2 coefficient in Eq. (3).

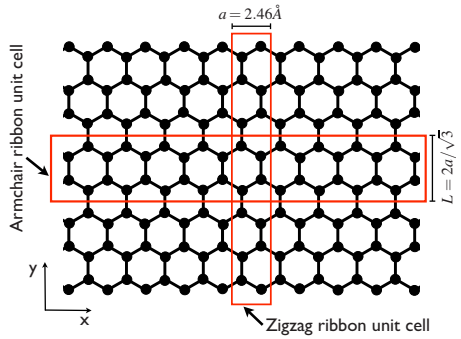

FIG. 5. (Color online) Representation of the unit-cell choices for armchair and zigzag edge-terminated graphene nanoribbons.

(a gap for charged excitations) at a density which depends on magnetic field. A gap at a field-dependent density necessarily[43,44] implies the presence of chiral edge states that support an equilibrium circulating current. The current varies with chemical potential at a rate defined by the field dependence of the bulk gap density. Most quantum-Hall measurements simply reflect the property[44] that separate local equilibria are established at opposite edges of a ribbon in systems with a bulk energy gap or mobility gap. It is immediately clear therefore that the $\nu=0$ quantum-Hall effect is special since it is due to an energy gap at the neutrality point, i.e., at a density which does not depend on magnetic field. The issue of whether or not the $\nu=0$ gap and associated phenomena should be referred to as an instance of the quantum-Hall effect is perhaps a delicate one. The $\nu=0$ gap is intimately related to Landau quantization and in this sense is comfortably grouped with quantum-Hall phenomena. This view supports the language we use in referring to the $\nu=0$ quantum-Hall effect. On the other hand, since it occurs at a field-independent density, its transport phenomena are more naturally viewed as those of an ordinary insulator[16] which just happens to be induced by an external magnetic field.

An exception occurs for the F state which does have edge states,[8,18] and can be viewed as having $\nu=1$ for majority spins and $\nu=-1$ for minority spins. In the simplest case, it has two branches of edge state with opposite chirality for opposite spin, much like those of quantum-spin-Hall[17] systems. In a Hall-bar geometry most transport measurements are very strongly sensitive to the presence or absence of edge states. In order to address edge-state physics directly at $\nu=0$ we have extended our study from the bulk graphene to the graphene nanoribbon case, Fig. 5. Tight-binding model solutions for a ribbon in the presence of a magnetic field can be obtained in essentially the same way as for bulk graphene, with the simplification that any magnetic-field strength preserves the one-dimensional ribbon wave vector k as a good quantum number when the gauge is chosen appropriately. This graphene ribbon problem in a magnetic field was studied time ago by Wakabayashi *et al.*[45] and revisited recently within both tight-binding[31,46] and continuum[8,47,48] models in order to provide a microscopic assessment of the relationship between Landau levels and edge states. The general feature of the ribbon band structure in the presence of a magnetic field is that those states localized near the edges have dispersive bands whereas those in the flat-band region are located mostly in the bulk. In the case of zigzag edge termination, edge localized states are present even in the absence of a magnetic field.[49] In the quantum-Hall regime these states are in the nondispersive band region such as the bulk localized states and they do not contribute to edge currents, although they can interact with other edge localized states.

Figure 6 explicitly illustrates how the character of the bulk broken symmetry is manifested in ribbon edge-state properties. Because of practical limitations our calculations are restricted to moderately narrow ribbons with widths of order 10 nm. In order to properly reproduce bulk Landau-level quantization in these narrow systems we have to choose magnetic-field strengths strong enough to yield magnetic lengths $\ell_B \sim 25\ \mathrm{nm}/(B[\mathrm{T}])^{1/2}$ substantially smaller than the ribbon width, i.e., fields stronger than typical experimental fields. On the other hand if the magnetic fields are too strong, say $\ell_B < a$ the levels will be strongly affected by the lattice and the properties of the solutions will substantially depart from the behavior we should expect at weaker magnetic fields, for which the continuum-model description is approximately correct. For field strengths in the appropriate range, we find the same three types of self-consistent field solutions as in the bulk calculations, namely, F, CDW, and SDW solutions. The band structures and spin-resolved densities presented in Fig. 6 confirm that only the F solution has states in the broken-symmetry-induced gap. Hall-bar transport properties for the F configuration have been discussed by Abanin *et al.*[8] and Fertig *et al.*[18] from a theoretical point of view. The CDW and SDW state electronic structure is insulating, both at the edge and in the bulk. The band structures of these two states are similar even though their spin-density profiles are quite distinct.

The plots of spin-↑ and spin-↓ partial densities across the ribbons hint at some of the physics which selects between the three candidate ordered states. In the truncated $n=0$ Landau-level continuum theory, the F state has one excess occupied Landau level for majority spins and one Landau level occupation deficiency for minority spins. We see in Fig. 6, that the size of these polarizations is not strongly influenced by the Landau-level mixing effects included in our lattice calculation. The $n=0$ continuum theory SDW state has the same spin excesses and deficiencies but they have opposite sign on opposite sublattices. We see in Fig. 6, that these order parameters are actually enhanced by Landau-level mixing effects; inter-Landau-level exchange effects polarize lower-energy occupied Landau-level states so that they enhance the SDW pattern. For the CDW state on the other hand, the $n=0$ Landau-level excess density on one sublattice is suppressed by Landau-level mixing. In this case the direct electrostatic interaction is nonzero so that the occupied Landau levels away from the Fermi energy are polarized between sublattices in the opposite sense of the $n=0$ levels. The fact that the SDW state is enhanced by Landau-level mixing explains why it is favored over the F state for the interaction parameters used to construct Fig. 6.

Finally, we comment on the microscopic electronic structure at the edges of an F state. As illustrated in Fig. 6, the mean-field electronic structure at the edge contains a domain wall.[18] Because textures in this domain wall can[18] carry charge, the F state edge is however not necessarily insulating

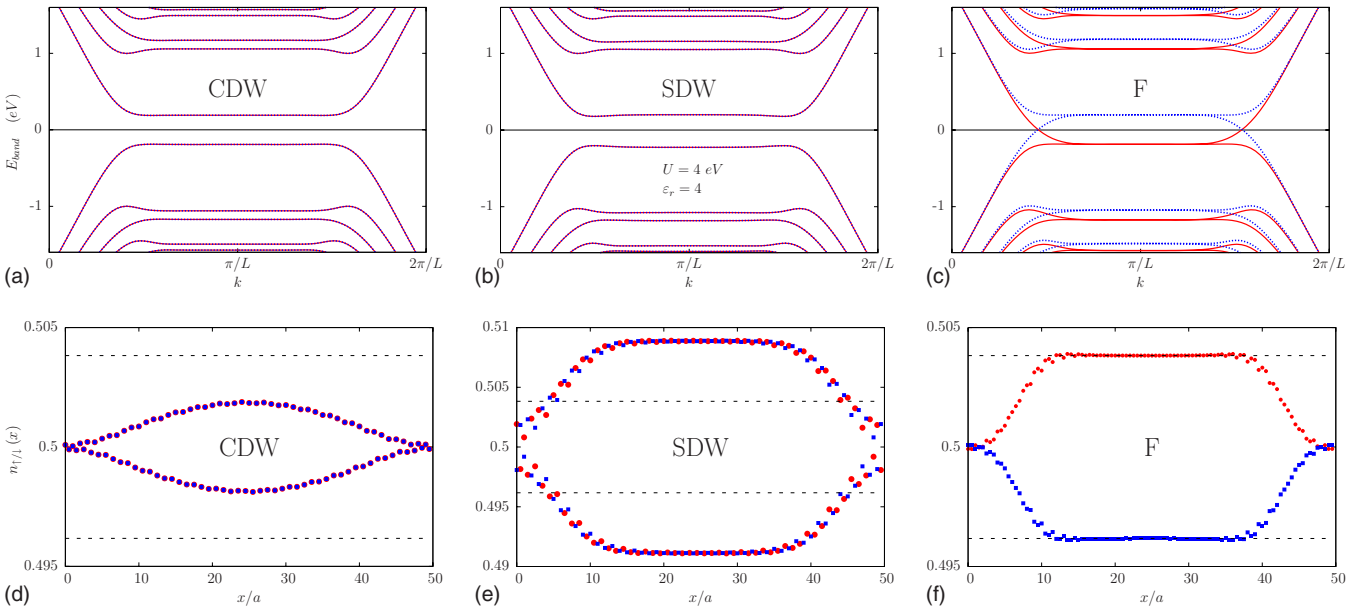

FIG. 6. (Color online) Band-structure and spin-density distributions in armchair ribbons calculated for $U=4$ eV and $\varepsilon_r=4$ for a magnetic field corresponding to $\ell_B=4.24a$ ($B=606$ T) using a 100×2 lattices in the unit cell and 80 k-point sampling in the Brillouin zone. The red color is used to represent up spin while blue is used for down spin. Upper row: Armchair ribbon band structures for the F, SDW, and CDW solutions. Only the F solution is metallic while the other two configurations are insulating. For this choice of parameters SDW is the energetically favored state but the energies of the other states are similar and their band gaps also have a similar size. Lower row: Spin-↑ and spin-↓ density distributions across one of the zigzag rows in the unit cell of an armchair ribbon. The influence of Landau-level mixing on the three solutions is apparent in the differences between the three sets of density distributions. In the case of SDW solutions Landau-level mixing enhances the local spin density while in the case of the CDW solution the magnitude of the charge-density oscillation is reduced by Landau-level mixing. The dashed horizontal lines represent the occupation in absence of Landau-level mixing.

in the absence of disorder. It was recently argued that impurities with magnetic moments near the sample edges can introduce spin-flip backscattering potentials[18] whose effectiveness is enhanced by the presence of a domain wall. The high resistances seen experimentally at $\nu=0$ therefore do not necessarily prove that the ground state is not an F state. The analysis in Ref. 18 was carried out within a Luttinger-liquid formalism whose parameters depend on the domain-wall shape. As illustrated in Fig. 7, our microscopic domain walls exhibit an interesting anisotropy in which inner and outer segments of the wall differ.

V. SUMMARY AND DISCUSSIONS

We have carried out a mean-field study of graphene's $\nu=0$ ground state which aims to shed light on the character of the interaction-induced gap that appears experimentally. The fact that the ground state has a charge gap at this filling factor can be established essentially rigorously[12] within the continuum model often used to describe graphene. When interaction-induced mixing between $n=0$ and $|n|\neq0$ Landau levels is neglected in the continuum model, the family of broken-symmetry states is related by arbitrary spin and valley pseudospin rotations and includes both fully spin-polarized F and spin (SDW) and charge (CDW) wave states. Our effort to determine the ground-state character when Landau-level mixing and lattice effects are included, is motivated by the observation of magnetic-field-induced insulating transport properties and by the expectation that transport properties in the quantum-Hall regime should be very different for F, SDW, and CDW states.

The lattice model we study has two phenomenological parameters, a relative dielectric constant ε_r and an on-site interaction parameter U. The most appropriate values of both parameters are somewhat uncertain. Our two main findings are that (i) Landau-level mixing effects favor the density-wave states over the ferromagnetic state and (ii) the competition between CDW and SDW states is sensitive to the relative strength of on-site and intersite electron-electron interactions and hence on the product $\varepsilon_r U$. Large values of this product increase the direct mean-field energy cost of CDW order and favor the SDW state. Exchange energies are stronger for density-wave states than for ferromagnetic states because order within the $n=0$ level, induces order in the full negative n Landau levels in the former case but not in the latter case. For graphene on SiO_2 and other typical substrates, sensible values for ε_r and U suggest that the field-induced state at $n=0$ is a SDW state. CDW states could occur in suspended graphene samples.

The atomic value of the on-site interaction term in carbon is $U\sim10$ eV so graphene values should be smaller. Most of the illustrative calculations we have described use either $U=4$ eV or $U=5$ eV. The dielectric constant is $\varepsilon_r\sim1$ for free-standing graphene. For a SiO_2 substrate, with dielectric constant $\varepsilon_r\sim4.5$, the effective 2D dielectric constant at a substrate/vacuum interface is $\varepsilon_r\sim2.5$. Because the Hartree-Fock approximation overestimates the strength of exchange interactions, it can be argued that somewhat larger values of

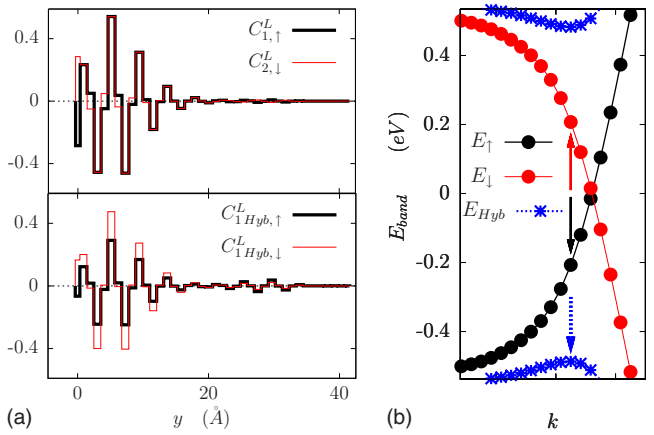

FIG. 7. (Color online) Quantum-hall edge domain-wall wave functions and energy bands corresponding to an F solution calculated for a zigzag graphene nanoribbon with 20 carbon atom pairs in the unit cell (W=42.6 Å) under a magnetic field of B=5660 T. Left panel: In the upper figure we represent the edge-state wave functions for the occupied and unoccupied ↑-spin and ↓-spin states when hybridization is not included. The lower figure represents the coefficients of the hybridized domain-wall state. All wave functions are plotted at the Bloch wave vector indicated by arrows on the right panel. Right panel: Quantum-hall edge-state bands with collinear-spin states represented by black and red symbols and the noncollinear-spin edge states formed by optimizing the hybridization of up- and down-spin orbitals represented by the blue symbols. We observe a clear single-particle energy gap related to the energy gained by forming the noncollinear domain-wall structure.

ε_r are appropriate—perhaps ~2 for free-standing graphene and $\varepsilon_r \sim 4$ or 5 for graphene on a substrate. Because of these uncertainties we view U and ε_r as effective parameters whose values are somewhat uncertain and have made energy comparisons over a wide range of values.

We are able to complete our calculations only at magnetic-field strengths much stronger than those available experimentally. Partly to verify that the field dependence is systematic, and partly in an effort to estimate the magnetic-field strengths necessary for Zeeman energies to drive the system into a F state, we have fit the energy differences between F and density-wave states to the form $\Delta E = C_{3/2}B^{3/2} + C_2 B^2$. Only the first term can be present for a continuum model with Coulomb interactions, and we find that this term is indeed dominant. We find that Zeeman coupling at typical fields can change the nature of the state only in the parameter range where the crossover from CDW to SDW states occurs. Although we assume collinear states in analyzing the SDW/F competition, we presume that the SDW to F crossover is actually a continuous one in which the antiparallel spins on opposite sublattices are smoothly rotated until they are aligned. Even if the bulk gap remains open the rotation of the spins will bring about a progressive closing of edge-state band gaps, until the gap is completely closed in the F configuration. The modulation of the edge charge gap due to Pauli paramagnetism might be detected in edge transport experiments. Since a relatively strong magnetic field is required to induce the insulating state in typical samples, we do not expect that it will be easy to produce parallel fields large enough to turn the system metallic while maintaining this minimum perpendicular field. Nevertheless, a study of the parallel-field dependence of transport properties is likely to hint at the nature of the underlying broken-symmetry state of the system.

All of these results ignore the influence of disorder. Experiments appear to show that the transition to the insulating state occurs at magnetic fields above some critical value that becomes smaller when the sample is cleaner. This is expected since disorder favors states without broken symmetries. The relationship between the minimum field and the mobility was carefully examined some time ago[6] but can be crudely described using the following simple argument. Assuming uncorrelated scatterers and using the Fermi golden rule the mobility is $\mu \propto 1/V_{dis}^2$, where V_{dis} is the typical energy scale of disorder. The crossover occurs when disorder strength equals the interaction energy scale $V_{dis}=U_{int} \propto B^{3/2}$, therefore the critical magnetic field between samples with different mobility are related through $B_c'/B_c=(\mu/\mu')^{1/3}$. One physical picture of the strong disorder limit asserts that current flows along domain walls which separate disorder-induced electron-hole puddles[16] domain walls along which current-carrying states with $\nu \neq 0$ can dominate bulk transport and suppress the divergent resistivity. In graphene on substrates the mobility values range between 2000 and 25 000 $cm^2\ V^{-1}\ s^{-1}$, and values as high as 230 000 $cm^2\ V^{-1}\ s^{-1}$ have been achieved in annealed suspended samples.[50] Typical critical fields in samples on substrates are in the 20–30 T range. From the above argument we can expect that the critical magnetic fields in suspended samples should be roughly two to five times lower.

An important goal of our work was to shed light on the character of the $\nu=0$ edge states. We examined the electronic structure of armchair ribbons with CDW, SDW, and F states, finding that edge states in the gap are absent for both CDW and SDW solutions. Given that the field-induced insulating state appears to have an *extremely* large resistance once established, it appears likely to us that the experimental state does not have edge states and that it therefore must be a density wave, as suggested by these calculations. If so, a study of the influence of magnetic-field tilting might be able to distinguish between SDW and CDW states.

ACKNOWLEDGMENTS

We acknowledge helpful discussions with R. Bistritzer, P. Cadden-Zimansky, Y. Zhao, K. Bolotin, F. Ghahari, P. Kim and financial support from Welch Foundation, NRI-SWAN, ARO, DOE, and the Spanish Ministry of Education through MEC-Fulbright program. We thank the assistance and computer hours provided by the Texas Advanced Computing Center (TACC).

[1] K. S. Novoselov, A. K. Geim, S. V. Morozov, D. Jiang, M. I. Katsnelson, I. V. Grigorieva, S. V. Dubonos, and A. A. Firsov, Nature (London) **438**, 197 (2005).
[2] Y. Zhang, Y.-W. Tan, H. L. Stormer, and P. Kim, Nature (London) **438**, 201 (2005).
[3] Y. Zhang, Z. Jiang, J. P. Small, M. S. Purewal, Y. W. Tan, M. Fazlollahi, J. D. Chudow, J. A. Jaszczak, H. L. Stormer, and P. Kim, Phys. Rev. Lett. **96**, 136806 (2006).
[4] S. M. Girvin and A. H. MacDonald, in *Perspectives in Quantum Hall Effects*, edited by S. Das Sarma and A. Pinczuk (John Wiley and Sons, New York, 1997).
[5] T. Jungwirth and A. H. MacDonald, Phys. Rev. B **63**, 035305 (2000).
[6] K. Nomura and A. H. MacDonald, Phys. Rev. Lett. **96**, 256602 (2006).
[7] J. Alicea and M. P. A. Fisher, Phys. Rev. B **74**, 075422 (2006); Solid State Commun. **143**, 504 (2007).
[8] D. A. Abanin, P. A. Lee, and L. S. Levitov, Phys. Rev. Lett. **96**, 176803 (2006); D. A. Abanin, K. S. Novoselov, U. Zeitler, P. A. Lee, A. K. Geim, and L. S. Levitov, *ibid.* **98**, 196806 (2007).
[9] J.-N. Fuchs and P. Lederer, Phys. Rev. Lett. **98**, 016803 (2007).
[10] I. F. Herbut, Phys. Rev. B **75**, 165411 (2007).
[11] M. O. Goerbig, R. Moessner, and B. Doucot, Phys. Rev. B **74**, 161407(R) (2006).
[12] K. Yang, S. Das Sarma, and A. H. MacDonald, Phys. Rev. B **74**, 075423 (2006).
[13] D. V. Khveshchenko, Phys. Rev. Lett. **87**, 206401 (2001); V. P. Gusynin, V. A. Miransky, S. G. Sharapov, and I. A. Shovkovy, Phys. Rev. B **74**, 195429 (2006).
[14] L. Sheng, D. N. Sheng, F. D. M. Haldane, and L. Balents, Phys. Rev. Lett. **99**, 196802 (2007).
[15] K. Nomura, S. Ryu, and D.-H. Lee, Phys. Rev. Lett. **103**, 216801 (2009).
[16] For a discussion of quantum-Hall insulating phase in bulk graphene see S. Das Sarma and K. Yang, Solid State Commun. **149**, 1502 (2009).
[17] C. L. Kane and E. J. Mele, Phys. Rev. Lett. **95**, 226801 (2005).
[18] H. A. Fertig and L. Brey, Phys. Rev. Lett. **97**, 116805 (2006); E. Shimshoni, H. A. Fertig, and G. V. Pai, *ibid.* **102**, 206408 (2009).
[19] I. Mihalek and H. A. Fertig, Phys. Rev. B **62**, 13573 (2000).
[20] D. A. Abanin, P. A. Lee, and L. S. Levitov, Phys. Rev. Lett. **98**, 156801 (2007).
[21] J. G. Checkelsky, Lu Li, and N. P. Ong, Phys. Rev. Lett. **100**, 206801 (2008).
[22] J. G. Checkelsky, Lu Li, and N. P. Ong, Phys. Rev. B **79**, 115434 (2009).
[23] A. J. M. Giesbers, L. A. Ponomarenko, K. S. Novoselov, A. K. Geim, M. I. Katsnelson, J. C. Maan, and U. Zeitler, Phys. Rev. B **80**, 201403 (2009).
[24] L. Zhang, J. Camacho, H. Cao, Y. P. Chen, M. Khodas, D. Kharzeev, A. Tsvelik, T. Valla, and I. A. Zaliznyak, arXiv:0904.1996 (unpublished).
[25] M. Amado, E. Diez, D. Lopez-Romero, F. Rossella, J. M. Caridad, V. Bellani, and D. K. Maude, arXiv:0907.1492 (unpublished).
[26] A. L. Tchougreeff and R. Hoffmann, J. Phys. Chem. **96**, 8993 (1992).
[27] J. G. Analytis, S. J. Blundell, and A. Ardavan, Am. J. Phys. **72**, 613 (2004).
[28] Y. Hasegawa and M. Kohmoto, Phys. Rev. B **74**, 155415 (2006).
[29] Y. Hasegawa, Y. Hatsugai, M. Kohmoto, and G. Montambaux, Phys. Rev. B **41**, 9174 (1990).
[30] L. Jiang and J. Ye, J. Phys.: Condens. Matter **18**, 6907 (2006).
[31] M. Arikawa, Y. Hatsugai, and H. Aoki, Phys. Rev. B **78**, 205401 (2008).
[32] A. H. Castro-Neto, F. Guinea, N. M. R. Peres, K. S. Novoselov, and A. K. Geim, Rev. Mod. Phys. **81**, 109 (2009).
[33] J. W. McClure, Phys. Rev. **104**, 666 (1956).
[34] R. Egger and A. O. Gogolin, Phys. Rev. Lett. **79**, 5082 (1997); M. Zarea and N. Sandler, *ibid.* **99**, 256804 (2007).
[35] P. P. Ewald, Ann. Phys. **369**, 253 (1921).
[36] P. J. Steinbach and B. R. Brooks, J. Comput. Chem. **15**, 667 (1994).
[37] J. Jung and A. H. MacDonald (unpublished).
[38] S. Dutta, S. Lakshmi, and S. K. Pati, Phys. Rev. B **77**, 073412 (2008).
[39] O. V. Yazyev, Phys. Rev. Lett. **101**, 037203 (2008).
[40] S. Bhowmick and V. B. Shenoy, J. Chem. Phys. **128**, 244717 (2008).
[41] B. Wunsch, T. Stauber, F. Sols, and F. Guinea, Phys. Rev. Lett. **101**, 036803 (2008).
[42] A. Szabo and N. Ostlund, *Modern Quantum Chemistry: Introduction to Advanced Electronic Structure Theory* (McGraw-Hill, New York, 1982).
[43] B. I. Halperin, Phys. Rev. B **25**, 2185 (1982).
[44] *Mesoscopic Quantum Physics*, edited by E. Akkermans, G. Montambeaux, J.-L. Pichard, and J. Zinn-Justin (Elsevier, Amsterdam, 1995).
[45] K. Wakabayashi, M. Fujita, H. Ajiki, and M. Sigrist, Phys. Rev. B **59**, 8271 (1999).
[46] Y. C. Huang, M. F. Lin, and C. P. Chang, J. Appl. Phys. **103**, 073709 (2008).
[47] L. Brey and H. A. Fertig, Phys. Rev. B **73**, 195408 (2006).
[48] V. P. Gusynin, V. A. Miransky, S. G. Sharapov, and I. A. Shovkovy, Phys. Rev. B **77**, 205409 (2008); V. P. Gusynin, V. A. Miransky, S. G. Sharapov, I. A. Shovkovy, and C. M. Wyenberg, Phys. Rev. B **79**, 115431 (2009).
[49] M. Fujita, K. Wakabayashi, K. Nakada, and K. Kusakabe, J. Phys. Soc. Jpn. **65**, 1920 (1996).
[50] K. I. Bolotin, K. J. Sikes, Z. Jiang, M. Klima, G. Fudenberg, J. Hone, P. Kim, and H. L. Stormer, Surf. Sci. **146**, 351 (2008).